AGU PUBLICATIONS

JGR

Journal of Geophysical Research: Earth Surface

RESEARCH ARTICLE
10.1002/2017JF004376

Effect of Topography on Subglacial Discharge and Submarine Melting During Tidewater Glacier Retreat

J. M. Amundson[1] **and D. Carroll**[2]

[1]Department of Natural Sciences, University of Alaska Southeast, Juneau, AK, USA, [2]Department of Earth Sciences, University of Oregon, Eugene, OR, USA

Key Points:
- We explored secular variations in subglacial discharge and submarine melting with an idealized model
- Subglacial discharge increases as tidewater glaciers retreat along retrograde beds
- Submarine melting depends on subglacial discharge and therefore promotes unstable retreat on retrograde beds

Correspondence to:
J. M. Amundson,
jmamundson@alaska.edu

Citation:
Amundson, J. M., & Carroll, D. (2018). Effect of topography on subglacial discharge and submarine melting during tidewater glacier retreat. *Journal of Geophysical Research: Earth Surface*, *123*, 66–79. https://doi.org/10.1002/2017JF004376

Received 25 MAY 2017
Accepted 29 NOV 2017
Accepted article online 7 DEC 2017
Published online 9 JAN 2018

Abstract To first order, subglacial discharge depends on climate, which determines precipitation fluxes and glacier mass balance, and the rate of glacier volume change. For tidewater glaciers, large and rapid changes in glacier volume can occur independent of climate change due to strong glacier dynamic feedbacks. Using an idealized tidewater glacier model, we show that these feedbacks produce secular variations in subglacial discharge that are influenced by subglacial topography. Retreat along retrograde bed slopes (into deep water) results in rapid surface lowering and coincident increases in subglacial discharge. Consequently, submarine melting of glacier termini, which depends on subglacial discharge and ocean thermal forcing, also increases during retreat into deep water. Both subglacial discharge and submarine melting subsequently decrease as glacier termini retreat out of deep water and approach new steady state equilibria. In our simulations, subglacial discharge reached peaks that were 6–17% higher than preretreat values, with the highest values occurring during retreat from narrow sills, and submarine melting increased by 14% for unstratified fjords and 51% for highly stratified fjords. Our results therefore indicate that submarine melting acts in concert with iceberg calving to cause tidewater glacier termini to be unstable on retrograde beds. The full impact of submarine melting on tidewater glacier stability remains uncertain, however, due to poor understanding of the coupling between submarine melting and iceberg calving.

1. Introduction

Subglacial discharge is a key component of tidewater glacier systems: it influences glacier dynamics by affecting basal friction (Kamb et al., 1994; Meier et al., 1994; Podrasky et al., 2012), it erodes and redistributes subglacial sediment (Cowan & Powell, 1991; Motyka et al., 2006), and it generates an upwelling plume that entrains warm ocean water (Straneo & Cenedese, 2014), melts glacier termini (Carroll et al., 2016; Slater et al., 2015), and drives a fjord-scale exchange flow (Carroll et al., 2015; Jackson & Straneo, 2016). As a result, fjord waters tend to be productive, nutrient-rich environments for plankton, fish, and sea birds (Arendt et al., 2016; Arimitsu et al., 2016; Lydersen et al., 2014; Meire et al., 2016; Urbanski et al., 2017). Variations in subglacial discharge likely affect the viability of these communities by impacting turbidity and nutrient concentrations.

Over seasonal and longer time scales, variations in subglacial discharge are clearly linked to changes in glacier volume (Jansson et al., 2003). Changes in surface elevation and surface area have opposing effects. For example, during retreat surface lowering promotes melting due to the dependence of temperature on elevation, whereas terminus retreat reduces the size of the glacier catchment (see Figure 1). Modeling studies suggest that for land-terminating glaciers, the net annual subglacial discharge during retreat can peak at values that are roughly 50% larger than preretreat values (Aðalgeirsdóttir et al., 2006; Huss et al., 2008); eventually, the subglacial discharge decreases to below preretreat values as the glaciers waste away or evolve to smaller steady state geometries. The relative change in subglacial discharge appears to depend strongly on climate type (maritime versus continental) (O'Neel et al., 2014) and is a function of climate change and basin hypsometry.

For land-terminating glaciers, the rates of surface lowering and terminus retreat are determined by two competing surface mass balance feedbacks: (i) a positive feedback loop with surface elevation and (ii) a negative feedback loop with glacier length (e.g., Harrison et al., 2001). These surface mass balance feedbacks also act on tidewater glaciers. However, additional feedbacks between glacier dynamics and frontal processes

Figure 1. Time-lapse photos from LeConte Glacier, Alaska, illustrating rapid terminus retreat, $\Delta L \sim -300$ m, and surface lowering, $\Delta H \sim -10$ m, that occurred during a 6 month period in 2016.

(i.e., iceberg calving, submarine melting, and sedimentation) can counteract the stabilizing feedback loop, causing tidewater glaciers to undergo decadal- to centennial-scale oscillations of slow advance and rapid retreat that can be asynchronous with climate (e.g., McNabb and Hock, 2014; Pfeffer, 2007; Post et al., 2011).

The ice-dynamic feedbacks that drive changes in tidewater glacier volume cause tidewater glacier termini to tend to be stable on seaward sloping beds and unstable on retrograde beds. This suggests that, by influencing the rate of volume change, subglacial topography must exert a strong control on secular variations in subglacial discharge. Here as a first step toward understanding these variations, we use an idealized, depth- and width-integrated glacier flow model to explore variations in subglacial discharge during retreat through a deep fjord. We further consider some of the consequences of this variability by coupling the flow model to an idealized line plume model.

2. Subglacial Discharge

Prior to describing the glacier flow model, we first develop a framework for exploring variations in subglacial discharge. Mass conservation dictates that the rate of change of water storage, S, in a basin containing a tidewater glacier is

$$\frac{dS}{dt} = P - ET - Q_s - Q_f, \tag{1}$$

where P and ET are the precipitation (solid plus liquid) and evapotranspiration fluxes, Q_s is stream discharge, and $Q_f > 0$ is the frontal ablation flux (iceberg calving plus submarine melting). For consistency all terms are expressed in ice equivalent units. If the glacier covers a large portion of the basin, then (i) Q_s equals the subglacial discharge Q_{sg}, (ii) evapotranspiration is a small component of the mass budget, especially over long time scales (Hock, 2005), and (ii) over annual and longer time scales, $dS/dt \approx dV/dt$, where V is the volume of the glacier. Thus, we ignore subglacial and englacial storage of water and, because supraglacial streams are rarely observed near the termini of tidewater glaciers, we also assume that all meltwater reaches the glacier bed and is evacuated subglacially. Under these conditions we are restricted to discussing secular variations in subglacial discharge.

The rate of change of glacier volume is

$$\frac{dV}{dt} = Q_b - Q_f, \tag{2}$$

where Q_b is the glacier-wide balance flux (sum of accumulation and ablation fluxes, including surface and basal processes; hereafter referred to as simply the "balance flux"). For simplicity, in our calculations we will assume that the balance flux is solely a result of surface processes but note that melt due to frictional heating and geothermal heat can account for up to ~20% of the subglacial discharge (Echelmeyer & Harrison, 1990). We later discuss the potential implications of frictional heating (see section 6).

Using the above approximations and combining equations (1) and (2) yields

$$Q_{sg} = P - Q_b = \int_{\Omega} (\dot{P} - \dot{B})\, \mathrm{d}\Omega, \tag{3}$$

where $\dot{P}$ and $\dot{B}$ are the precipitation and specific mass balance rates (in meters per year of ice equivalent) and Ω is the glacier surface area. For tidewater glaciers a large fraction of the precipitation that falls over the basin exits the glacier at the terminus via submarine melting and iceberg calving and not as subglacial discharge; thus, the subglacial discharge will generally be less than the precipitation flux. In other words, unlike land-terminating glaciers, the balance flux is generally positive (even during retreat) for tidewater glaciers and does not approach zero as a glacier evolves toward a steady state.

Since we are interested in what drives the variability in subglacial discharge, we take the derivative of equation (3) while applying the Leibniz integral rule, which gives

$$\frac{\mathrm{d}Q_{sg}}{\mathrm{d}t} = \int_{\Omega} \left(\frac{\partial \dot{P}}{\partial h} - \frac{\partial \dot{B}}{\partial h} \right) \frac{\partial h}{\partial t}\, \mathrm{d}\Omega + (\dot{P}_t - \dot{B}_t) W_t \frac{\mathrm{d}L}{\mathrm{d}t}, \tag{4}$$

where h is the glacier surface elevation, $\dot{P}_t$ and $\dot{B}_t$ are the width-averaged precipitation and specific mass balance rates at the terminus, W_t is the terminus width, and L is the glacier length. In deriving equation (4) we have assumed that changes in surface area occur primarily due to changes in glacier length, which is in line with our depth- and width-averaged flow model (section 3). Equation (4) illustrates that the rate of change of subglacial discharge depends on (i) climate type (e.g., maritime versus continental) and variability (changes in precipitation and/or mass balance rate) and (ii) glacier dynamics, which determines the rates of change of surface elevation and glacier length. The first term on the right-hand side accounts for the evolution of the glacier surface and is positive during retreat because surface lowering enhances melting, whereas the second term accounts for the change in drainage basin size and is negative during retreat due to a decrease in the precipitation flux. The rate of length change, $\mathrm{d}L/\mathrm{d}t$, depends on iceberg calving and submarine melting; however, the physical mechanisms driving these processes remain poorly understood. In our model simulations we therefore use an idealized parameterization for the rate of length change (section 3.3) and test the model sensitivity to the choice of that parameterization.

3. Model Description

We use a one-dimensional, depth- and width-integrated flow model (Enderlin et al., 2013; Nick et al., 2009) to explore the variability of subglacial discharge during tidewater glacier retreat through a deep fjord. We focus on modeling retreat because terminus advance through deep water is difficult to sustain without the development and progradation of an end moraine (e.g., Amundson, 2016; Nick et al., 2007); including a moraine component in the model would introduce additional uncertainty. We chose to use a simplified flow model instead of a more accurate higher-order model because it allows us to rapidly identify the key processes driving variations in subglacial discharge from a large number of hypothetical subglacial topographies.

3.1. Model Domain

The model domain and climate are designed to mimic temperate tidewater glaciers in Alaska. The domain consists of a large accumulation area that funnels ice into a narrow, deep fjord containing a shallow sill and/or narrow lateral constriction. The bed elevation, h_b, was prescribed as the sum of two Gaussian bumps, one which describes the overall background topography and another that describes the width and height of the sill:

$$h_b = 2.4e^{-\frac{(x+10)^2}{2*40^2}} + h_s e^{-\frac{(x-100)^2}{2w_s^2}} - 0.4, \tag{5}$$

where h_s and w_s are the sill height and root-mean-square (RMS) sill width (in kilometers). Later, we present our results in terms of the sill depth (distance from the ocean surface to the top of the sill). A similar function was used to prescribe the glacier width, W:

$$W = 8e^{-\frac{x^2}{2*25^2}} + h_w e^{-\frac{(x-100)^2}{2w_c^2}} + 4, \tag{6}$$

where h_w is the constriction amplitude and w_c is the RMS width of the constriction. We ran simulations in which we (i) varied the shape of the sill and did not include a constriction and (ii) included a constriction but no sill; see Figures 2a, 2b, 3a, and 3b for examples of the model domain.

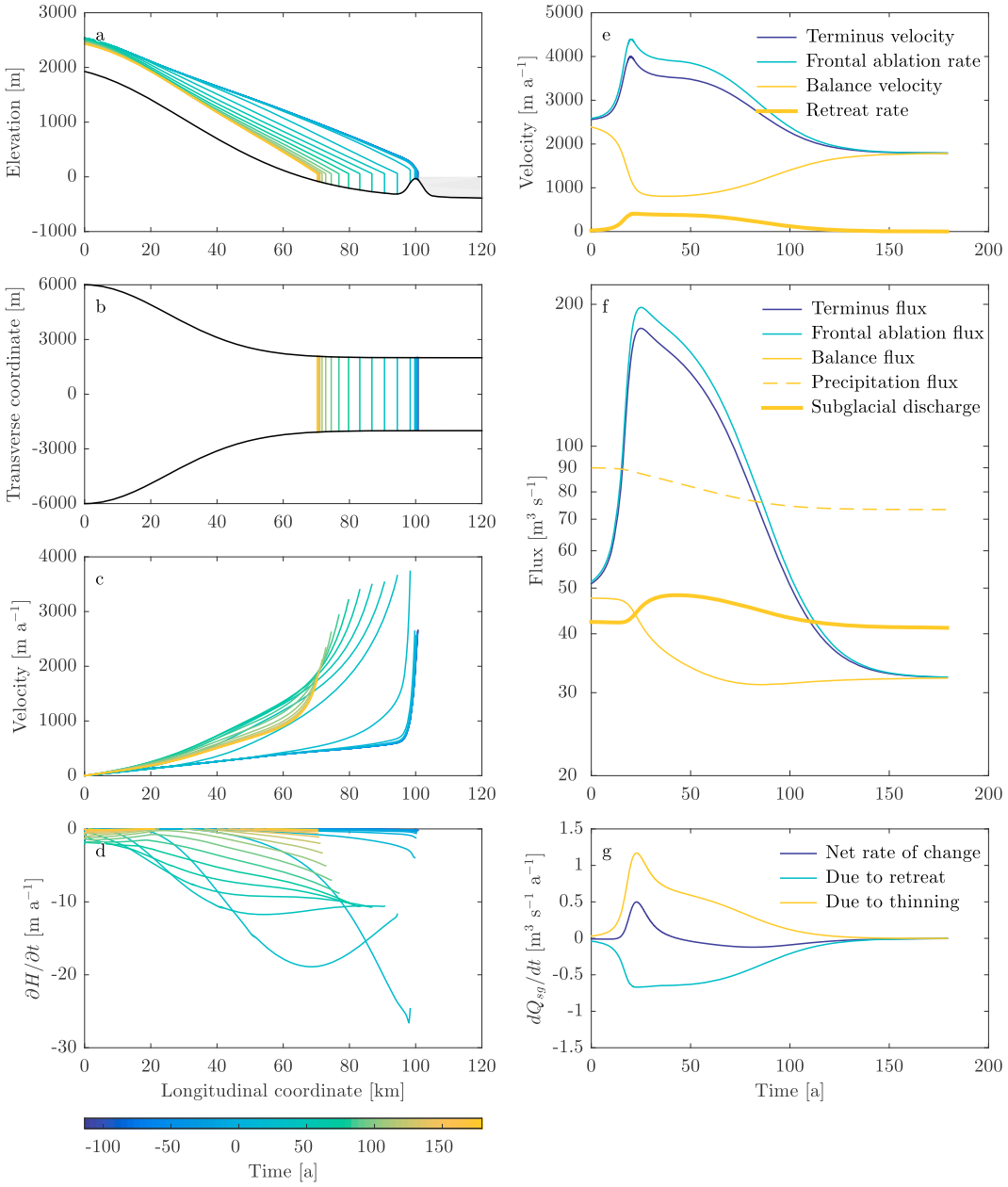

Figure 2. Terminus retreat from a sill that is 30 m deep and has a RMS width of 2,000 m. $t = 0$ corresponds to the time at which the terminus retreats past the highest point of the sill. Evolution of (a) glacier surface elevation, (b) glacier length, (c) longitudinal velocity profile, and (d) thinning rate. Profiles are 10 years apart. Temporal variations in (e) velocities and (f) fluxes (note the logarithmic scale). (g) Variations in subglacial discharge are partitioned into components due to retreat and due to thinning (see equation (4)).

Climate is prescribed using a mass balance profile that varies linearly with altitude until reaching a maximum accumulation rate, such that

$$\dot{B}(z) = \min\left(\frac{\mathrm{d}\dot{B}}{\mathrm{d}z}(z - z_{\mathrm{ELA}}),\ \dot{B}_{\mathrm{max}}\right), \tag{7}$$

where $\mathrm{d}\dot{B}/\mathrm{d}z = 0.01$ a^{-1} is the mass balance gradient, z is elevation, and z_{ELA} is the elevation of the equilibrium line altitude (ELA). We set $\dot{B}_{\mathrm{max}} = 4$ m a^{-1}. This climate parameterization was designed to roughly mimic glaciers in southern Alaska (e.g., Motyka et al., 2002; Van Beusekom et al., 2010). The mass balance gradient and maximum accumulation rate would both be lower for glaciers in more continental or polar climates

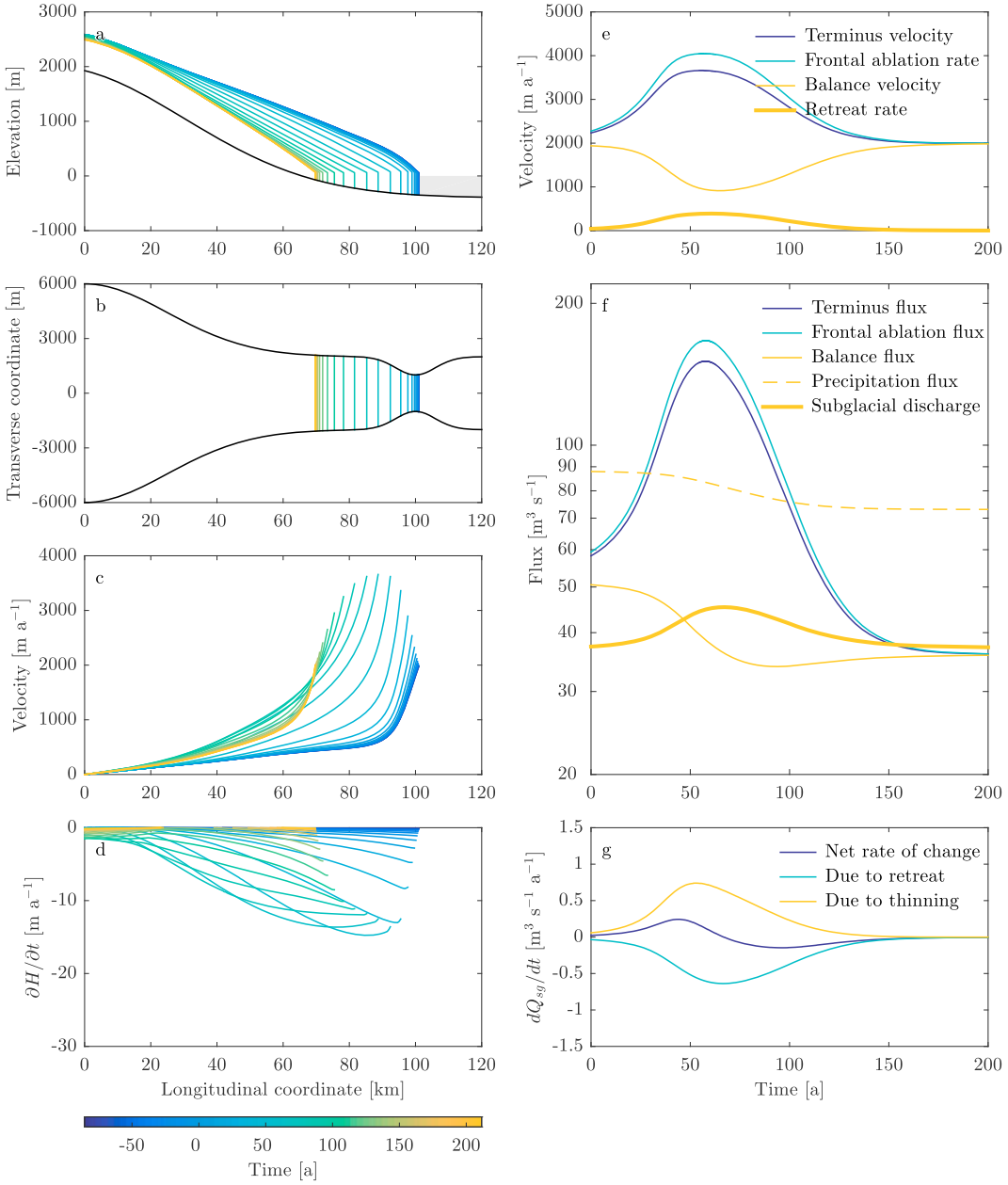

Figure 3. Terminus retreat from a constriction that narrows to 2,000 m. $t = 0$ corresponds to the time at which the terminus retreats past the narrowest point of the constriction. Evolution of (a) glacier surface elevation, (b) glacier length, (c) longitudinal velocity profile, and (d) thinning rate. Profiles are 10 years apart. Temporal variations in (e) velocities and (f) fluxes (note the logarithmic scale). (g) Variations in subglacial discharge are partitioned into components due to retreat and due to thinning (see equation (4)).

(Cuffey & Paterson, 2010). Calculations of subglacial discharge require both the balance flux, which is calculated from the balance profile and the glacier hypsometry, and the precipitation flux. For simplicity, we calculate the precipitation flux by prescribing a constant precipitation rate over the entire glacier that is equal to the maximum balance rate (i.e., $\dot{P} = 4$ m a^{-1}).

3.2. Governing Equations and Boundary Conditions

Ice flow is modeled using conservation of momentum, which requires that the glaciological driving stress is balanced by gradients in longitudinal stress, basal drag, and lateral drag (van der Veen, 2013), such that

$$2\frac{\partial}{\partial x}\left[H\nu\frac{\partial U}{\partial x}\right] - \beta N\,|U|^{-\frac{2}{3}}\,U - \frac{2H}{W}\left(\frac{5}{AW}\right)^{\frac{1}{3}}|U|^{-\frac{2}{3}}\,U = \rho_i g H\frac{\partial h}{\partial x}, \tag{8}$$

where H is ice thickness, β is the basal roughness factor, N is effective basal pressure, A is the flow rate factor, $\rho_i = 917\,\mathrm{kg\,m^{-3}}$ is ice density, g is gravitational acceleration, and ν is the depth-averaged effective viscosity, defined as

$$\nu = A^{-\frac{1}{3}} \left| \frac{\partial U}{\partial x} \right|^{-\frac{2}{3}}. \tag{9}$$

We use a constant flow rate factor of $A = 2.4 \times 10^{-24}\,\mathrm{Pa^{-3}s^{-1}}$, consistent with low-latitude tidewater glaciers (Cuffey & Paterson, 2010), and a constant basal roughness factor of $\beta = 1.78\,\mathrm{s^{1/3}m^{-1/3}}$, which yields basal resistance coefficients $\beta N |U|^{-\frac{2}{3}}$ that range from $\sim 10^{11}$ Pa s m^{-1} at the divide to close to 0 at the terminus (see also Enderlin et al., 2013). The effective pressure is calculated by defining a linear phreatic surface that starts at the glacier bed at the divide and decreases to sea level at the terminus. The minimum permitted effective pressure is 0, which occurs if part of the glacier goes afloat; note that this did not occur during our simulations.

A Dirichlet boundary condition is used to prescribe a velocity of $U = 0$ at the divide ($x = 0$) and a Neumann boundary condition to prescribe the velocity gradient at the terminus (see equation (11) below). The depth-integrated, longitudinal deviatoric stress, σ'_{xx}, at the terminus is found by subtracting the depth-integrated hydrostatic pressure from the depth-integrated glaciostatic pressure, giving

$$\sigma'_{xx}\Big|_{x=L} = \frac{1}{2}\rho_i g \left(H - \frac{\rho_w}{\rho_i}\frac{D^2}{H} \right), \tag{10}$$

where $\rho_w = 1{,}028\,\mathrm{kg\,m^{-3}}$ is the density of sea water and D is the submerged depth of the terminus. Inserting equation (10) into Glen's Flow law gives

$$\frac{\partial U}{\partial x}\Big|_{x=L} = A \left[\frac{\rho_i g}{4} \left(H - \frac{\rho_w}{\rho_i}\frac{D^2}{H} \right) \right]^3. \tag{11}$$

At each time step the glacier surface is evolved by applying the calculated velocities and a prescribed mass balance profile to a depth- and width-integrated mass continuity equation, in which

$$\frac{\partial H}{\partial t} = \dot{B} - \frac{1}{W}\frac{\partial (UHW)}{\mathrm{d}x}. \tag{12}$$

Further details of the numerical method used to solve these equations are presented in Enderlin et al. (2013).

3.3. Parameterization of the Rate of Length Change

During the model simulations the glacier terminus position is adjusted using the mass flux parameterization of the rate of length change introduced in Amundson (2016). The parameterization is based on the observation that, over long time scales, terminus retreat is associated with surface lowering and flow acceleration, while terminus advance is associated with thickening and slow flow. This suggests that the rate of volume change is related to the imbalance between the balance flux and the ice flux through the terminus, Q_t. We thus assume that

$$\frac{\mathrm{d}V}{\mathrm{d}t} = f(Q_b - Q_t). \tag{13}$$

Using a first-order Taylor's series expansion yields

$$\frac{\mathrm{d}V}{\mathrm{d}t} = f(0) + \frac{f'(0)}{1!}(Q_b - Q_t) + \ldots \approx \alpha(Q_b - Q_t). \tag{14}$$

Equating equations (2) and (14) yields

$$Q_b - Q_f = \alpha(Q_b - Q_t). \tag{15}$$

Data from Jakobshavn Isbræ, Helheim Glacier, and Kangerdluggsuaq Glacier support a linear relationship between $Q_b - Q_f$ and $Q_b - Q_t$, with a best fit slope of $\alpha = 1.14$ and a slope uncertainty of 0.03 (Amundson, 2016; Howat et al., 2011). We use that value as a starting point and also consider the model sensitivity to the choice of α. Rearranging equation (15) and dividing by the cross-sectional area of the terminus gives

$$\frac{\mathrm{d}L}{\mathrm{d}t} = U_t - U_f = (\alpha - 1)(U_b - U_t), \tag{16}$$

where U_f is the frontal ablation rate and U_b and U_t are the terminus balance velocity and depth- and width-averaged terminus velocity. We use equation (16) to update the terminus position after each time step.

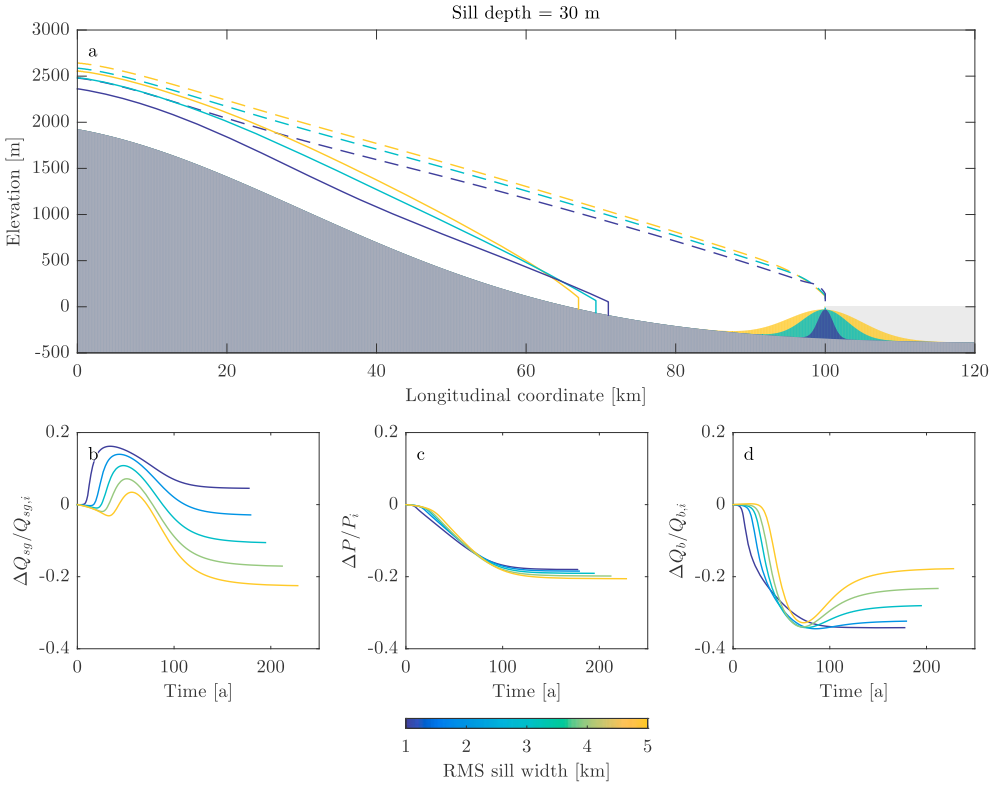

Figure 4. Variations in subglacial discharge for varying sill widths. Colors correspond to the RMS width of the sill. (a) Glacier geometry at time $t = 0$ (when the terminus passes over the sill; dashed lines) and when the glacier reaches its final steady state configuration (solid lines). (b–d) Fractional changes in subglacial discharge, precipitation flux, and balance flux; the initial values at $t = 0$ are indicated by subscript i.

Ultimately, the mass flux parameterization relates the rate of length change to the mean rate of thinning or thickening. Although the parameterization is heuristic, it is developed from mass continuity arguments and observations of tidewater glacier advance and retreat over annual and longer time scales. The parameterization is robust for both floating and grounded termini and produces unstable advance/retreat along retrograde beds (as demonstrated in Amundson, 2016).

3.4. Numerical Simulations

The model is first spun-up to a steady state, defined as occurring when the rate of advance or retreat is less than 1 m a^{-1}. During spin-up the terminus is free to advance or retreat; if the glacier does not reach a steady state with the terminus located on the seaward side of the sill/constriction (i.e., if $L < 100$ km), then the ELA is lowered by 50 m and spin-up is restarted. Due to the highly nonlinear behavior of ice flow, particularly for tidewater glaciers, small changes in bedrock topography or numerical model parameters can produce large differences in glacier geometry. As a result we spun-up simulations with a wide range of ELAs (from ~700 to 1,300 m, with narrow sills requiring lower ELAs than wide sills) in order to produce initial steady state solutions for a variety of different bedrock topographies. Consequently, the initial fluxes varied slightly between simulations. Retreat from the initial steady state solution is triggered by incrementally raising the ELA by 10 m until the glacier begins an unstable retreat through the fjord after which the ELA is held constant; simulations are halted when the terminus reaches a new steady state.

To investigate the effect of topography on variations in subglacial discharge, we ran the model for a variety of sill and constriction geometries. In the majority of our simulations we did not include a constriction and therefore focused on the effect of subglacial topography. Sill depths and RMS sill widths were varied from 10 to 50 m and from 1 to 5 km, respectively. Additional simulations without a sill were used to test the effect of lateral constrictions; below we present results from a single experiment in which we generated a constriction that narrowed to 2 km (at $x = 100$ km) and had a RMS width of 6 km.

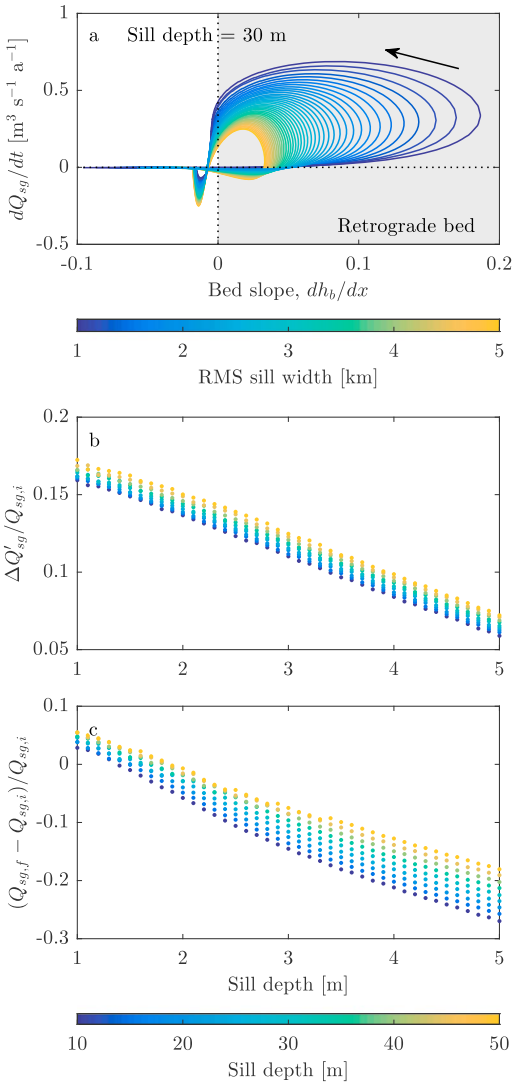

Figure 5. Comparison of subglacial discharge peak and net change in subglacial discharge for sill depths ranging from 10–50 m and RMS sill widths ranging from 1 to 5 km. (a) Rate of change of subglacial discharge versus bed slope at the terminus. The gray shaded region indicates where the bed has a retrograde slope. (b) Peak subglacial discharge amplitude relative to the subglacial discharge at $t = 0$. (c) Relative change in subglacial discharge from time $t = 0$ to the final steady state geometry (indicated by subscripts *i* and *f*).

In addition to investigating the effect of topography, we also tested the effect of model parameters on glacier behavior. We varied the frontal ablation factor α by 3% (1.11–1.17; based on the uncertainty in the best fit value of α from Amundson, 2016) and the basal resistance factor β by 6% (1.67–1.89 s$^{1/3}$ m$^{-1/3}$) from their initial values. Varying β more than about 6% produced glaciers with accumulation areas that were unrealistically thin or thick.

4. Results

Our model produced rapid retreat through the roughly 30 km long fjord. The simulations generally lasted 200–300 years, with the majority of retreat occurring in a 100 year time span. Model results were similar for simulations with (i) a sill but no constriction and (ii) a constriction but no sill (Figures 2 and 3). Velocities, rates of retreat, fluxes, and variations in these parameters were all of similar magnitude. For simplicity we hereafter focus on describing the model behavior during retreat along a retrograde bed but note that retreat from a constriction produces similar behavior. The fastest retreat rates, which were on the order of 300 m a^{-1}, coincided with high velocities and rapid thinning and occurred as the terminus was retreating into deep water (Figures 2c–2e). In all simulations the subglacial discharge increased during retreat into deep water, in some cases by up to 15–20% (Figures 2f and 4). This indicates that dynamic thinning that occurs during retreat down a retrograde bed has a larger impact on subglacial discharge than does the reduction in drainage basin size (Figure 2g). After reaching deep water the retreat rates remain high but the thinning rate decreases, and consequently, the subglacial discharge also decreases.

The rate at which subglacial discharge increases during retreat into deep water depends indirectly on bed slope, with higher slopes (narrower sills) producing a faster rate of change (Figure 5a). The hysteresis in Figure 5a is indicative of a lag between the bed slope at the terminus and the change in subglacial discharge and is observed because surface lowering occurs in response to a loss of basal resistance (i.e., buttressing force from the sill) (see also Pfeffer, 2007). The size of the peak in subglacial discharge, $\Delta Q'_{sg}$, increases with decreasing sill width and increasing sill depth (Figure 5b) because short, narrow sills provide the least resistance to glacier flow, which allows for rapid drawdown during retreat into deep water. For most simulations, there is an overall net reduction in subglacial discharge (Figure 5c) due to a reduction in the drainage basin size. However, if the thinning rates are high enough, the corresponding reduction in balance flux will offset the reduction in precipitation flux and the net change in subglacial discharge may be slightly positive. For example, a 1 km wide sill produced peak and final steady state subglacial discharges that were 17% and 4% greater than the initial subglacial discharge (depending on sill depth); for a 5 km wide sill these values were 7% and −20% (Figure 5). The variability in subglacial discharge is controlled primarily be the evolving surface mass balance and less so by the evolving precipitation flux (Figure 4).

Simulations with a single fixed bedrock topography are used to explore the sensitivity of these results to model parameters (Figure 6). Lowering the basal resistance factor β results in higher peak rates of retreat, more rapid thinning, and a larger peak in subglacial discharge. Changing the frontal ablation factor, α, has a different and larger effect. A higher value of α results in a faster rate of retreat and a higher rate of thinning but a reduced peak in subglacial discharge. These differences occur because the basal resistance has a larger impact on the first term in equation (4) (increase in surface melting due to dynamic thinning) than on the second term (reduction in drainage basin size), whereas changing α has a larger impact on the second term.

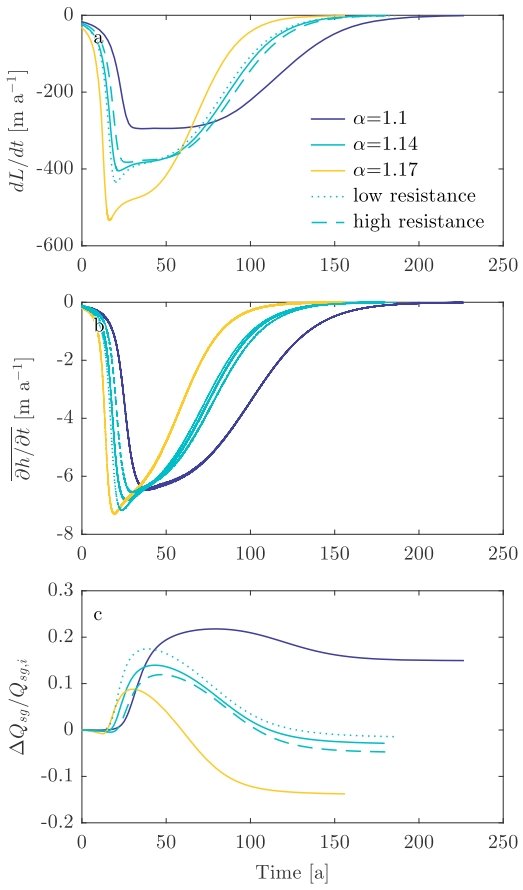

Figure 6. Dependence of model results on the frontal ablation factor, α, and the basal roughness factor, β. The basal roughness factor was set to 1.78 (s/m)$^{1/3}$ (solid lines), 1.67 (s/m)$^{1/3}$ (dotted lines), and 1.89 (s/m)$^{1/3}$ (dashed lines). In these simulations the sill is 30 m deep and has a RMS width of 2,000 m. Colors represent different parameter combinations. (a and b) Variations in retreat rate and the mean rate of thinning. (c) Fractional changes in subglacial discharge relative to the initial subglacial discharge at $t = 0$ (indicated by subscript i).

This is consistent with the notion that sill geometry influences subglacial discharge primarily by affecting flow resistance.

The evolution of glacier geometry, and therefore subglacial discharge, is ultimately determined by the relationship between the rates of length and thickness change. These processes are linked in parameterizations of calving through the longitudinal strain rate, which affects both fracture propagation (e.g., van der Veen, 1998a, 1998b) and the rate of thickness change (see equation (12)). Moreover, the rate of thickness change is sensitive to the parameterization of basal motion (see Benn et al., 2007). Testing various combinations of basal sliding relationships and calving parameterizations is beyond the scope of this study, but we note that the general pattern of retreat produced by our model (i.e., rapid retreat and surface lowering during retreat along a retrograde bed) is consistent with other modeling studies (e.g., Nick et al., 2009; Schoof, 2007).

5. Implications for Submarine Melting

Submarine melting is an important driver of tidewater glacier dynamics. Direct observations of submarine termini (Fried et al., 2015; Rignot et al., 2015) and numerical models (Slater et al., 2017) show that meltwater plumes enhance undercutting of grounded glacier termini, representing a mechanism for increased calving (Luckman et al., 2015; O'Leary & Christoffersen, 2013) and potential glacier destabilization (Nick et al., 2009). Previous work has demonstrated that submarine melt rates scale with subglacial discharge and ocean temperature. For example, Jenkins (2011) showed that for low subglacial discharge and weak stratification,

$$\dot{m} \propto Q_{sg}^{1/3}(T_a - T_f), \tag{17}$$

where Q_{sg} is now expressed in water equivalent units, $\dot{m}$ is the melt rate near the grounding line, and $T_a - T_f$ is the ocean thermal forcing (ambient ocean temperature minus the pressure-salinity-dependent freezing point). This scaling relationship appears to be consistent with field observations from Southeast Alaska (e.g., Motyka et al., 2013). Our model results therefore imply that, due to the dependence on subglacial discharge, submarine melt rates should increase during retreat along retrograde beds and decrease during retreat up seaward sloping beds.

5.1. Coupled Glacier-Plume Simulations

As a first step toward assessing long time scale variations in submarine melting and its consequences for glacier dynamics, we couple our one-dimensional ice flow model with the idealized line plume model of Jenkins (2011). The plume model takes fjord stratification and subglacial discharge as input and calculates melt rates as a function of depth. We treat the maximum melt rate, which occurs near the grounding line, as a proxy for undercutting (see also Rignot et al., 2016) and use it to modify the frontal ablation factor α in the equation for the rate of length change (equation (16)). This modification is perhaps understood most easily by solving equation (16) for the depth- and width-averaged calving rate. Noting that $dL/dt = U_t - U_c - U_m$, where U_c and U_m are the depth- and width-averaged calving and submarine melt rates, and rearranging, gives

$$U_c = \alpha U_t + (1 - \alpha)U_b - U_m. \tag{18}$$

Equation (18) indicates that changes in calving rate are strongly affected by changes in terminus velocity U_t and weakly affected by changes in balance velocity U_b (because $\alpha \approx 1.14$). Submarine melting can affect the parameterized calving rate by (i) removing ice that would otherwise calve off of the glacier (via U_m), which by itself does not affect the rate of length change, (ii) directly affecting the terminus balance velocity and ice velocity for glaciers that terminate with ice shelves (the entire glacier was always grounded in our simulations),

and (iii) promoting calving via undercutting. We allow for the latter by using an ad hoc assumption that α varies linearly with the maximum submarine melt rate calculated by the plume model, such that

$$\alpha = 1.14 + 5 \times 10^{-5}(\dot{m} - \dot{m}_i), \tag{19}$$

where $\dot{m}_i$ is the initial submarine melt rate. This formulation ensures that the initial value of α is 1.14 for all simulations. In our simulations, the submarine melt rate varied by about 300 m a^{-1} (depending on fjord stratification), and therefore, α varied by a few percent (ranged at most from 1.137 to 1.155).

The plume model parameters follow Jenkins (2011); submarine melt rate is calculated using the three-equation thermodynamic model described in Holland and Jenkins (1999). The plume model assumes that subglacial discharge is distributed across the entire width of the terminus. Although highly idealized, this line plume model is similar to point source formulations (Cowton et al., 2015) in that the submarine melt rate is strongly related to subglacial discharge and thermal forcing; it is therefore adequate for our purposes and is consistent with our depth- and width-integrated glacier flow model.

We use idealized fjord temperature and salinity profiles, representative of typical summer stratification in Alaska fjords (e.g., Motyka et al., 2003), with the analytic forms

$$T(z) = \Re(T_o + \Delta T(z/z_o)^\gamma) \tag{20}$$

and

$$S(z) = \Re(S_o + \Delta S(z/z_o)^\gamma), \tag{21}$$

where $\Re$ refers to the real part of the functions in parentheses, $T_o = 4°C$ and $S_o = 28$ are the initial surface temperature and salinity (in practical salinity scale), ΔT and ΔS are the increase in temperature and salinity from the surface to 400 m depth, $z < 0$ is the depth, and $z_0 = 50$ m is the pycnocline depth. The exponent γ was set to 1/3. We considered three different fjord profiles (Figure 7): (i) constant temperature and salinity with depth ($\Delta T = 0$ and $\Delta S = 0$), (ii) continuous stratification with depth ($\Delta T = 0$ and $\Delta S = 0$), which would represent efficient fjord renewal processes (e.g., Arneborg et al., 2004; Mortensen et al., 2011), and (iii) the same as (ii) but with constant temperature and salinity below the top of the sill.

5.2. Variations in Submarine Melting

As expected, the submarine melt rate increases in all coupled model simulations ($\alpha = f(\dot{m})$) as the terminus retreats into deep water, which also results in a faster rate of retreat than in the uncoupled model simulations ($\alpha \neq f(\dot{m})$) (Figures 7a and 7b). Interestingly, the submarine melt rates are slightly lower in the coupled simulations than in the uncoupled simulations because the faster rate of retreat in the coupled simulations does not provide as much time for surface lowering. Thus, there is a slight reduction in peak subglacial discharge when compared to the uncoupled simulations.

Although we ran the full plume model, we verified a posteriori that the scaling between submarine melting, subglacial discharge, and ocean thermal forcing (equation (17)) is valid for the subglacial discharge and fjord properties in our simulations. Taking the derivative of equation (17) in order to express the rate of change of the maximum submarine melt rate in terms of the rates of change of subglacial discharge and ocean thermal forcing yields

$$\frac{\mathrm{d}\dot{m}}{\mathrm{d}t} \propto \frac{1}{3} Q_{sg}^{-2/3}(T_a - T_f)\frac{\mathrm{d}Q_{sg}}{\mathrm{d}t} + Q_{sg}^{1/3}\frac{\mathrm{d}T_a}{\mathrm{d}t} - Q_{sg}^{1/3}\frac{\mathrm{d}T_f}{\mathrm{d}t}. \tag{22}$$

Plotting each of the terms in equation (22) separately (Figure 7d), we find that the rate of change of submarine melting is strongly affected by changes in ambient ocean temperature (which is an approximately linear function of depth for the second of our three fjord profiles) and weakly affected by changes in the pressure-salinity-dependent freezing point and subglacial discharge. Importantly, all three of these terms represent positive feedbacks that enhance retreat down retrograde beds.

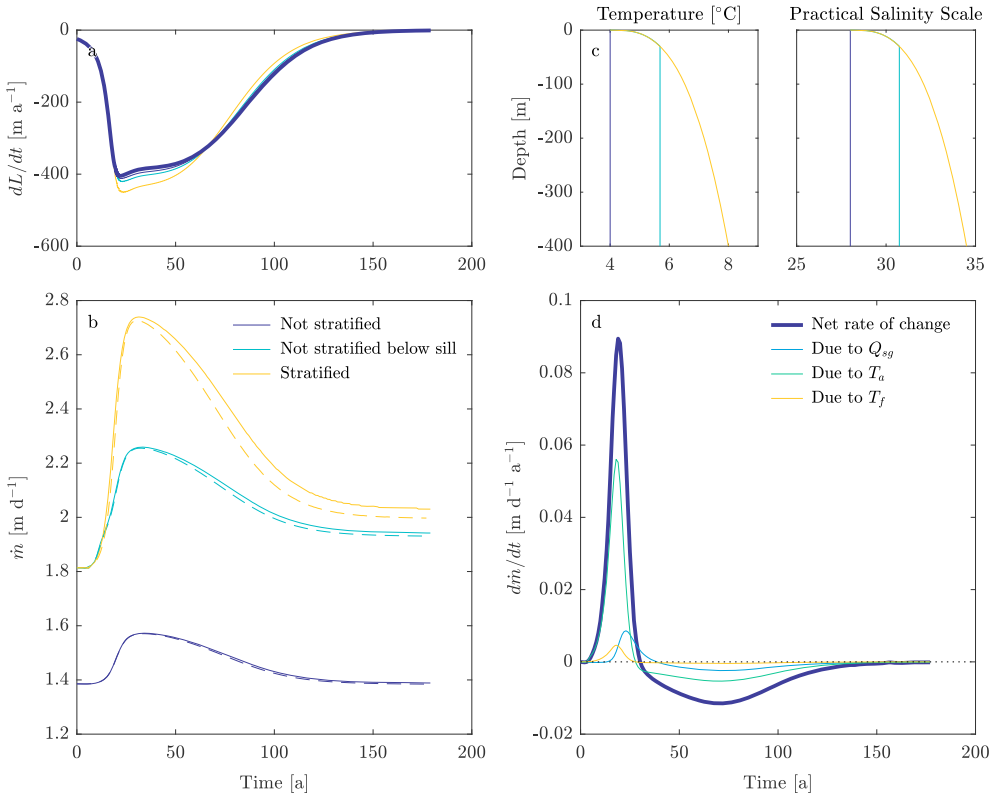

Figure 7. Modeled maximum submarine melt rates (which occur near the grounding line) and retreat rates for uncoupled and coupled simulations. The sill is 30 m deep and has a RMS width of 2,000 m. Colors represent different fjord stratifications. (a) Comparison of retreat rate in the uncoupled simulation (thick blue line) to retreat rates in the coupled simulations. (b) Maximum calculated submarine melt rates (with respect to depth) using the line plume model for uncoupled (solid lines) and coupled (dashed lines) simulations. (c) Temperature and salinity profiles used in the simulations. (d) Net rate of change of submarine melting and components due to variations in subglacial discharge, ambient ocean temperature, and pressure-salinity freezing point at the base of the terminus for the stratified simulation (dashed yellow line in Figure 7b).

6. Discussion and Conclusions

Tidewater glacier retreat is in some ways analogous to the erosion of an earthen dam. As a dam erodes there is an imbalance between the fluxes into and out of the reservoir. The faster the erosion occurs, the greater this imbalance and the faster the reservoir surface will drop. Similar behavior is observed for tidewater glaciers. Retreat into deep water (or past a lateral constriction) results in an imbalance between the balance flux and the ice flux. This imbalance similarly causes a drawdown of the glacier surface, with the rate of surface lowering affected by the sill geometry. However, the imbalance also affects the volume of the reservoir (i.e., the glacier) by indirectly removing ice from both the surface and the terminus. Surface lowering brings the ice into warmer elevations where surface melt can proceed more quickly, but it also reduces the effective pressure and enhances ice velocities, strain rates, and calving activity, thereby causing the basin size to decrease. Competition between these indirect effects determines the evolution of subglacial discharge. The dynamic thinning that occurs during tidewater glacier retreat, and its impact on subglacial discharge, distinguishes tidewater glaciers from land-terminating glaciers.

During retreat into deep water (or past a lateral constriction), surface lowering dominates and subglacial discharge increases by up to about 15–20%, even in a steady climate. As the terminus retreats through the fjord and begins to restabilize, terminus retreat dominates the change in subglacial discharge, and eventually, the subglacial discharge may decrease to below its preretreat value. The relative magnitudes of the variations in subglacial discharge are sensitive to bedrock topography. The largest peaks occur for glaciers that retreat off of narrow, deep sills, because these sills provide the least amount of flow resistance. Surface lowering

becomes less important as sill width increases; glaciers that retreat off of wide sills experience smaller peaks in subglacial discharge during retreat into deep water and experience a larger overall reduction in subglacial discharge.

A key consequence of our modeling study is that submarine melting tends to increase when tidewater glaciers retreat down retrograde beds. Submarine melt rates depend strongly on subglacial discharge, ambient ocean temperature, and the pressure-salinity freezing point of ice. All three of these properties contribute to an increase in submarine melt rates as a terminus retreats into deep water. Variations in ambient ocean temperature appear to have the largest impact on submarine melt rates, with subglacial discharge and the pressure-salinity freezing point having secondary and comparable effects. Thus, our results suggest that tidewater glacier termini are unstable on retrograde beds due to both mechanical and thermodynamic processes (i.e., calving and submarine melting). The net effect of submarine melting on terminus stability remains poorly constrained, however, due to poor understanding of both the relationship between submarine melting and iceberg calving and the processes that control ocean heat transport in fjords.

We did not account for some processes that may enhance the relative impact of subglacial discharge on submarine melting. First, the model assumed a steady climate. Detailed modeling studies of land-terminating glaciers suggest that subglacial discharge from those glaciers will initially increase by 25–50% under various climate warming scenarios (Aðalgeirsdóttir et al., 2006; Huss et al., 2008) before decreasing to preretreat values. Tidewater glaciers that retreat in a warming climate should be expected to experience similar climate-driven variations in subglacial discharge in addition to the glacier-dynamic-driven variations described here. Second, our model ignored frictional heating as a source of meltwater. Estimates from Jakobshavn Isbræ, Greenland, suggest that frictional heating may account for 20% of the glacier's subglacial discharge (Echelmeyer & Harrison, 1990). Frictional heating scales with the product of the shear stress and the velocity and should therefore also increase during retreat down a retrograde bed.

Our model was highly idealized and designed to illustrate the basic feedbacks between terminus retreat, surface lowering, and subglacial discharge. Due to the highly nonlinear dynamics of glacier flow, seasonal and shorter-period variability in climate (including feedbacks due to changing surface topography), subglacial hydrology, iceberg calving, and submarine melting may have significant consequences for long-period evolution of tidewater glaciers and fjord ecosystems. Future work should attempt to analyze the impact of short-term variability in these processes, as is similarly being done for land-terminating glaciers (e.g., Roe & Baker, 2014), and should also investigate secular variations in subglacial discharge and submarine melting for glaciers in a larger variety of settings (see Truffer & Motyka, 2016).

Acknowledgments
Funding was provided by the National Oceanic and Atmospheric Association (NA13OAR4310098) and the U.S. National Science Foundation (PLR-1504288 and PLR-1504521). We thank scientific Editor B. Hubbard, P.-M. Lefeuvre, and two anonymous reviewers for comments that improved the clarity of the manuscript. Model code used in this manuscript can be accessed through the Arctic Data Center (http://doi.org/10.18739/A21K1Q); model output is available by contacting the corresponding author (jmamundson@alaska.edu).

References

Aðalgeirsdóttir, G., Jóhannesson, T., Björnsson, H., Pálsson, F., & Sigurðsson, O. (2006). Response of Hofsjökull and southern Vatnajökull, Iceland, to climate change. *Journal of Geophysical Research*, *111*, F03001. https://doi.org/10.1029/2005JF000388

Amundson, J. M. (2016). A mass-flux perspective of the tidewater glacier cycle. *Journal of Glaciology*, *62*(231), 82–93. https://doi.org/10.1017/jog.2016.14

Arendt, K., Dalgaard Agersted, M., Sejr, M., & Juul-Pedersen, T. (2016). Glacial meltwater influences on plankton community structure and the importance of top-down control (of primary production) in a NE Greenland fjord. *Estuarine, Coastal and Shelf Science*, *183*, 123–135. https://doi.org/10.1016/j.ecss.2016.08.026

Arimitsu, M., Piatt, F., & Mueter, F. (2016). Influence of glacier runoff on ecosystem structure in Gulf of Alaska fjords. *Marine Ecology Progress Series*, *560*, 19–40. https://doi.org/10.3354/meps11888

Arneborg, L., Erlandsson, C. P., Liljebladh, B., & Stigebrandt, A. (2004). The rate of inflow and mixing during deep-water renewal in a sill fjord. *Limnology and Oceanography*, *49*(3), 768–777. https://doi.org/10.4319/lo.2004.49.3.0768

Benn, D. I., Hulton, N. R. J., & Mottram, R. H. (2007). "Calving laws", "sliding laws" and the stability of tidewater glacier. *Annals of Glaciology*, *46*, 123–130.

Carroll, D., Sutherland, D. A., Hudson, B., Moon, T., Catania, G. A., Shroyer, E. L., … van den Broeke, M. R. (2016). The impact of glacier geometry on meltwater plume structure and submarine melt in Greenland fjords. *Geophysical Research Letters*, *43*, 9739–9748. https://doi.org/10.1002/2016GL070170

Carroll, D., Sutherland, D. A., Shroyer, E. L., Nash, J. D., Catania, G. A., & Stearns, L. A. (2015). Modeling turbulent subglacial meltwater plumes: Implications for fjord-scale buoyancy-driven circulation. *Journal of Physical Oceanography*, *45*, 2169–2185. https://doi.org/10.1175/JPO-D-15-0033.1

Cowan, E., & Powell, R. (1991). Ice-proximal sediment accumulation rates in a temperate glacial fjord, southeastern Alaska. *GSA Special Papers*, *261*, 61–74. https://doi.org/10.1130/SPE261-p61

Cowton, T., Slater, D., Sole, A., Goldberg, D., & Nienow, P. (2015). Modeling the impact of glacial runoff on fjord circulation and submarine melt rate using a new subgrid-scale parameterization for glacial plumes. *Journal of Geophysical Research: Oceans*, *120*, 796–812. https://doi.org/10.1002/2014JC010324

Cuffey, K. M., & Paterson, W. S. B. (2010). *The physics of glaciers* (4th ed.). Amsterdam: Elsevier.

Echelmeyer, K., & Harrison, W. D. (1990). Jakobhavns Isbræ, West Greenland: Seasonal variations in velocity—or lack thereof. *Journal of Glaciology*, *36*(122), 82–88.

Enderlin, E., Howat, I., & Vieli, A. (2013). High sensitivity of tidewater outlet glacier dynamics to shape. *Cryosphere*, *7*, 1007–1015. https://doi.org/10.5194/tc-7-1007-2013

Fried, M. J., Catania, G. A., Bartholomaus, T. C., Duncan, D., Davis, M., Stearns, L. A., … Sutherland, D. (2015). Distributed subglacial discharge drives significant submarine melt at a Greenland tidewater glacier. *Geophysical Research Letters*, *42*, 9328–9336. https://doi.org/10.1002/2015GL065806

Harrison, W., Elsberg, D., Echelmeyer, K., & Krimmel, R. (2001). On the characterization of glacier response by a single time-scale. *Journal of Glaciology*, *47*(159), 659–664.

Hock, R. (2005). Glacier melt: A review of processes and their modelling. *Progress in Physical Geography*, *29*(3), 362–391.

Holland, D., & Jenkins, A. (1999). Modeling thermodynamic ice-ocean interactions at the base of an ice shelf. *Journal of Physical Oceanography*, *29*, 1787–1800.

Howat, I. M., Ahn, Y., Joughin, I., van den Broeke, M. R., Lenaerts, J. T. M., & Smith, B. (2011). Mass balance of Greenland's three largest outlet glaciers, 2000–2010. *Geophysical Research Letters*, *38*, L12501. https://doi.org/10.1029/2011GL047565

Huss, M., Farinotti, D., Bauder, A., & Funk, M. (2008). Modelling runoff from highly glacierized alpine drainage basins in a changing climate. *Hydrological Processes*, *22*, 3888–3902. https://doi.org/10.1002/hyp.7055

Jackson, R. H., & Straneo, F. (2016). Heat, salt and freshwater budgets for a glacial fjord in Greenland. *Journal of Physical Oceanography*, *46*, 2735–2768.

Jansson, P., Hock, R., & Schneider, T. (2003). The concept of glacier storage: A review. *Journal of Hydrology*, *282*, 116–129. https://doi.org/10.1016/S0022-1694(03)00258-0

Jenkins, A. (2011). Convection-driven melting near the grounding lines of ice shelves and tidewater glaciers. *Journal of Physical Oceanography*, *41*, 2279–2294.

Kamb, B., Engelhardt, H., Fahnestock, M. A., Humphrey, N., Meier, M., & Stone, D. (1994). Mechanical and hydrologic basis for the rapid motion of a large tidewater glacier: 2. Interpretation. *Journal of Geophysical Research*, *99*(B8), 15,231–15,244. https://doi.org/10.1029/94JB00467

Luckman, A., Benn, D. I., Cottier, F., Bevan, S., Nilsen, F., & Inall, M. (2015). Calving rates at tidewater glaciers vary strongly with ocean temperature. *Nature Communications*, *6*, 8566. https://doi.org/10.1038/ncomms9566

Lydersen, C., Assmy, P., Falk-Petersen, S., Kohler, J., Kovacs, K. M., Reigstad, M., … Zajaczkowski, M. (2014). The importance of tidewater glaciers for marine mammals and seabirds in Svalbard, Norway. *Journal of Marine Systems*, *129*, 452–471. https://doi.org/10.1016/j.jmarsys.2013.09.006

McNabb, R., & Hock, R. (2014). Alaska tidewater glacier terminus positions, 1948–2012. *Journal of Geophysical Research: Earth Surface*, *119*, 153–167. https://doi.org/10.1002/2013JF002915

Meier, M., Lundstrom, S., Stone, D., Kamb, B., Engelhardt, H., Humphrey, N., … Walters, R. (1994). Mechanical and hydrologic basis for the rapid motion of a large tidewater glacier: 1. Observations. *Journal of Geophysical Research*, *99*(B8), 15,219–15,229. https://doi.org/10.1029/94JB00237

Meire, L., Meire, P., Struyf, E., Krawczyk, D. W., Arendt, K. E., Yde, J. C., … Meysman, F. J. R. (2016). High export of dissolved silica from the Greenland Ice Sheet. *Geophysical Research Letters*, *43*, 9173–9182. https://doi.org/10.1002/2016GL070191

Mortensen, J., Lennert, K., Bendtsen, J., & Rysgaard, S. (2011). Heat sources for glacial melt in a sub-Arctic fjord (Godthåbsfjord) in contact with the Greenland Ice Sheet. *Journal of Geophysical Research*, *116*, C01013. https://doi.org/10.1029/2010JC006528

Motyka, R. J., Dryer, W. P., Amundson, J. M., Truffer, M., & Fahnestock, M. (2013). Rapid submarine melting driven by subglacial discharge, LeConte Glacier, Alaska. *Geophysical Research Letters*, *40*, 5153–5158. https://doi.org/10.1002/grl.51011

Motyka, R. J., Hunter, L., Echelmeyer, K. A., & Connor, C. (2003). Submarine melting at the terminus of a temperate tidewater glacier, LeConte Glacier, Alaska, U.S.A. *Annals of Glaciology*, *36*, 57–65.

Motyka, R. J., O'Neel, S., Connor, C. L., & Echelmeyer, K. A. (2002). Twentieth century thinning of Mendenhall Glacier, Alaska, and its relationship to climate, lake calving, and glacier run-off. *Global and Planetary Change*, *35*, 93–112.

Motyka, R. J., Truffer, M., Kuriger, E. M., & Bucki, A. K. (2006). Rapid erosion of soft sediments by tidewater glacier advance: Taku Glacier, Alaska, USA. *Geophysical Research Letters*, *33*, L24504. https://doi.org/10.1029/2006GL028467

Nick, F. M., van der Veen, C. J., Vieli, A., & Benn, D. I. (2007). Controls on advance of tidewater glaciers: Results from numerical modeling applied to Columbia Glacier. *Journal of Geophysical Research*, *112*, F03S24. https://doi.org/10.1029/2006JF000551

Nick, F. M., Vieli, A., Howat, I. M., & Joughin, I. (2009). Large-scale changes in Greenland outlet glacier dynamics triggered at the terminus. *Nature Geoscience*, *2*, 110–114. https://doi.org/10.1038/ngeo394

O'Leary, M., & Christoffersen, P. (2013). Calving on tidewater glaciers amplified by submarine frontal melting. *Cryosphere*, *7*, 119–128. https://doi.org/10.5194/tc-7-119-2013

O'Neel, S., Hood, E., Arendt, A., & Sass, L. (2014). Assessing streamflow sensitivity to variations in glacier mass balance. *Climatic Change*, *123*, 329–341. https://doi.org/10.1007/s10584-013-1042-7

Pfeffer, W. (2007). A simple mechanism for irreversible tidewater glacier retreat. *Journal of Geophysical Research*, *112*, F03S25. https://doi.org/10.1029/2006JF000590

Podrasky, D., Truffer, M, Fahnestock, M., Amundson, J. M., Cassotto, R., & Joughin, I. (2012). Outlet glacier response to forcing over hourly to interannual timescales, Jakobshavn Isbræ, Greenland. *Journal of Glaciology*, *58*(212), 1212–1226. https://doi.org/10.3189/2012JoG12J065

Post, A., O'Neel, S., Motyka, R. J., & Streveler, G. (2011). A complex relationship between calving glaciers and climate. *Eos, Transactions American Geophysical Union*, *92*(37), 305–307.

Rignot, E., Fenty, I., Xu, Y., Cai, C., & Kemp, C. (2015). Undercutting of marine-terminating glaciers in West Greenland. *Geophysical Research Letters*, *42*, 5909–5917. https://doi.org/10.1002/2015GL064236

Rignot, E., Xu, Y., Menemenlis, D., Mouginot, J., Scheuchl, B., Li, X., … de Fleurian, B. (2016). Modeling of ocean-induced ice melt rates of five West Greenland glaciers over the past two decades. *Geophysical Research Letters*, *43*, 6374–6382. https://doi.org/10.1002/2016GL068784

Roe, G. H., & Baker, M. B. (2014). Glacier response to climate perturbations: An accurate linear geometric model. *Journal of Glaciology*, *60*(222), 670–684. https://doi.org/10.3189/2014JoG14J016

Schoof, C. (2007). Ice sheet grounding line dynamics: Steady states, stability, and hysteresis. *Journal of Geophysical Research*, *112*, F03S28. https://doi.org/10.1029/2006JF000664

Slater, D. A., Nienow, P. W., Cowton, T. R., Goldberg, D. N., & Sole, A. J (2015). Effect of near-terminus subglacial hydrology on tidewater glacier submarine melt rates. *Geophysical Research Letters*, *42*, 2861–2868. https://doi.org/10.1002/2014GL062494

Slater, D. A., Nienow, P. W., Goldberg, D. N., Cowton, T. R., & Sole, A. J. (2017). A model for tidewater glacier undercutting by submarine melting. *Geophysical Research Letters*, *44*, 2360–2368. https://doi.org/10.1002/2016GL072374

Straneo, F., & Cenedese, C. (2014). The dynamics of Greenland's glacial fjords and their role in climate. *Annual Review of Marine Science*, *7*(1), 89–112. https://doi.org/10.1146/annurev-marine-010213-135133

Truffer, M., & Motyka, R. J. (2016). Where glaciers meet water: Subaqueous melt and its relevance to glaciers in various settings. *Reviews of Geophysics*, *54*, 220–239. https://doi.org/10.1002/2015RG000494

Urbanski, J. A., Stempniewicz, L., Węsławski, J. A., Dragańska-Deja, K., Wochna, A., Goc, M., & Iliszko, L. (2017). Subglacial discharges create fluctuating foraging hotspots for sea birds in tidewater glacier bays. *Scientific Reports*, *7*, 43999. https://doi.org/10.1038/srep43999

Van Beusekom, A. E., O'Neel, S. R., March, R. S., Sass, L. C., & Cox, L. H. (2010). Re-analysis of Alaska benchmark glacier mass-balance data using the index method (Report 2010-5247): USGS Scientific Investigations.

van der Veen, C. J. (1998a). Fracture mechanics approach to penetration of surface crevasses on glaciers. *Cold Regions Science and Technology*, *27*(1), 31–47.

van der Veen, C. J. (1998b). Fracture mechanics approach to penetration of bottom crevasses on glaciers. *Cold Regions Science and Technology*, *27*(3), 213–223.

van der Veen, C. J. (2013). *Fundamentals of glacier dynamics* (2nd ed.). Boca Raton, FL: CRC Press.